



# CHORUS

This is the accepted manuscript made available via CHORUS. The article has been published as:

## Phase stability of the SrMnO<sub>3</sub> hexagonal perovskite system at high pressure and temperature

Morten Bormann Nielsen, Davide Ceresoli, Paraskevas Parisiades, Vitali B. Prakapenka, Tony Yu, Yanbin Wang, and Martin Bremholm

Phys. Rev. B **90**, 214101 — Published 1 December 2014

DOI: [10.1103/PhysRevB.90.214101](https://doi.org/10.1103/PhysRevB.90.214101)

# Phase stability of the SrMnO<sub>3</sub> hexagonal perovskite system at high pressure and temperature

Morten Bormann Nielsen<sup>\*</sup>, Davide Ceresoli<sup>†</sup>, Paraskevas Parisiades<sup>‡</sup>,  
Vitali B. Prakapenka<sup>§</sup>, Tony Yu<sup>§</sup>, Yanbin Wang<sup>§</sup>, Martin Bremholm<sup>\*,□</sup>

<sup>\*</sup> *Center for Materials Crystallography (CMC), Department of Chemistry and iNANO, Aarhus University, Langelandsgade 140, 8000 Aarhus C, Denmark*

<sup>†</sup> *Center for Materials Crystallography and Institute of Molecular Science and Technology (CNR-ISTM), via Golgi 19, 20133 Milano, Italy*

<sup>‡</sup> *European Synchrotron Radiation Facility, Beamline ID27, 71 Avenue des Martyrs, CS 40220, 38043, Grenoble Cedex 9, France*

<sup>§</sup> *Center for Advanced Radiation Sources, The University of Chicago, 5640 S. Ellis Ave., Chicago, IL 60637, USA*

□ *Corresponding author. Email: [bremholm@chem.au.dk](mailto:bremholm@chem.au.dk)*

## Abstract

SrMnO<sub>3</sub> is a perovskite compound which, unlike most perovskites, can be synthesized in three different but closely related polymorphs. In this paper, the first experimental equation of state of the 6H polymorphs is reported. The experimentally determined bulk modulus of SrMnO<sub>3</sub> increases from 115.6(11) GPa in the 4H polymorph to 143.7(17) GPa in the 6H polymorph, while DFT calculations predict a further increase to 172.5(4) GPa in the 3C polymorph. The first *in situ* observations of transformations between the three known polymorphs, under high pressure and high temperature conditions are also reported. The results are compared with extensive DFT calculations and literature, and it is demonstrated that the 6H polymorph is the thermodynamically stable phase between 5.9(3) and 18.1(2) GPa at zero kelvin. The effect of possible oxygen sub-stoichiometry is also explored, used DFT. Finally, the findings are combined with the existing knowledge of the phase behavior in this system to outline where further knowledge needs to be collected before a PT phase diagram can be constructed for this system.

## I. INTRODUCTION

Inorganic compounds with the formula  $ABX_3$  very often crystallize in the well-known perovskite structure, or distorted derivatives thereof. In the ideal cubic structure, the unit cell can be described by an  $AX_3$  cubic close-packed layer, with B ions in the octahedral holes that are surrounded only by X anions. The packing sequence is  $abc$ ,  $a$  being the first hexagonal layer,  $b$  the second layer that covers half the holes in  $a$ , and  $c$  the third placed on top of  $b$  to cover the other half. This class of materials covers a wide range of technologically relevant compounds that can display piezoelectric<sup>1</sup>, ferroelectric<sup>2</sup>, (anti)ferromagnetic<sup>3</sup>, catalytic<sup>4</sup>, semiconducting<sup>5</sup>, metallic<sup>6</sup> or insulating<sup>6</sup> behavior. Due to the widespread use of materials with this structure, it is worthwhile trying to gain a deeper insight into the factors governing phase stability in this type of system.

Many cases are known where A is either an alkaline earth metal or a lanthanoid while B is a transition metal. In these compounds, the B cation dominates the resulting physical properties, while the A ion is less important (except for the case of magnetic properties if a lanthanoid is used). The A ion, however, has a large influence on whether and how the crystal structure is distorted from the cubic structure. Quite often, the type of distortion can be predicted by the basic Goldschmidt tolerance factor<sup>7</sup>,  $t$ , which can be calculated from ionic radii,  $r$ , by equation 1.

$$t = \frac{r_A + r_X}{\sqrt{2}(r_B + r_X)} \quad (1)$$

When this value is between roughly 0.9 and 1, the structure found is often corner-sharing with small distortions from the ideal cubic perovskite. If the A ion is too small, tilts of octahedra occur for  $t < 0.9$ , serving to reduce the coordination number of A. The resulting structures are often orthorhombic or, as  $t$  decreases past 0.85, of the  $\text{LiNbO}_3$  and later ilmenite types<sup>8</sup>. On the other hand, when A is too large and  $t > 1$ , face-sharing of octahedra is commonly observed along with unit cells of hexagonal symmetry.

Many of the distorted perovskites transform to the cubic phase when subjected to high temperatures. The effect of high pressure is subtly different. While there are several examples of the cubic phase being induced by pressure<sup>9</sup>, other times the effect of pressure is to distort structures even more (e.g. the post-perovskite transition in  $\text{MgSiO}_3$ <sup>10</sup>). Another possibility is transformations that only bring the structure a bit closer to cubic.  $\text{BaMnO}_3$  is one example of such a compound. The ambient phase displays a hexagonal close-packing ( $ab$  stacking of the hexagonal layers as described above) of  $\text{BaO}_3$  with Mn located in the center of face-sharing octahedra. This polymorph is named 2H since each unit cell contains two close-packed layers along the  $c$ -axis of the unit cell and the symmetry is hexagonal. Syono *et al.*<sup>9</sup> were the first to report that when subjected to high pressure, the packing changes towards cubic close-packed in two steps. The first step is the 9H-phase with the packing sequence ( $ababcbcac$ ), while the second step is the 4H-phase with the packing sequence ( $abac$ ). Again the naming scheme follows the number of close packed layers in the unit cell and the symmetry.

The above series of transformations can be rationalized in terms of the tolerance factor (calculated throughout this paper using SPuDs<sup>11</sup> and the revised Shannon-Prewitt crystal ionic radii<sup>12</sup>): Ba<sup>2+</sup> is too large to produce the ideal corner-sharing structure at ambient pressure ( $t = 1.10$ ), but when subjected to high pressures, this ion is more compressible than Mn<sup>4+</sup> and O<sup>2-</sup>, producing a smaller  $t$ . At 3 GPa and 1123 K, the 9H phase becomes favored and at even higher pressure and temperature, 9 GPa and 1473 K, the 4H phase becomes favored<sup>9</sup>.

When Ba<sup>2+</sup> is exchanged for the smaller Sr<sup>2+</sup>, a marked decrease in the tolerance factor results,  $t = 1.04$ . It is therefore not surprising that 4H-SrMnO<sub>3</sub> (being closer to the ideal structure) is the thermodynamically stable phase at ambient conditions. Its unit cell can be seen in Fig. 1(a). The fact that the corner-sharing (cubic, 3C) polymorph can be stabilized to ambient conditions (through a non-stoichiometric synthesis route discovered by Negas and Roth<sup>13</sup>) showcases how the 0.9-1.0 cubic range is merely a generalized rule and how clever synthesis routes can be used to end up in metastable phase regions. Following the same line of reasoning as for BaMnO<sub>3</sub>, it would be expected that 4H-SrMnO<sub>3</sub> transforms to 3C-SrMnO<sub>3</sub> if subjected to pressure. The 3C-SrMnO<sub>3</sub> unit cell is shown in Fig. 1(b). Recently, Søndena *et al.*<sup>5</sup> determined the equation of state (EoS) of 4H-SrMnO<sub>3</sub> up to 40 GPa and used comparisons with DFT calculations on both 4H- and 3C-SrMnO<sub>3</sub> to argue that the latter should be more stable above 12 GPa. However, no such transition has been observed to date.

For BaMnO<sub>3</sub>, Syono *et al.*<sup>9</sup> reported the transformation of 4H-SrMnO<sub>3</sub> at 5 GPa and 1123 K into a new hexagonal phase which they determined to contain six formula units. They proposed that this new phase was isostructural with the high temperature 6H-BaTiO<sub>3</sub>, which displays the packing sequence (*abcacb*). The existence of this phase was not discussed in the study by Søndena *et al.*<sup>5</sup>, possibly because it was only recently solved by synchrotron powder x-ray diffraction (SR-PXRD) by Belik *et al.*<sup>14</sup> In the latter study, it was confirmed that the structure of the high pressure phase is of the 6H type. This unit cell is seen in Fig. 1(c) To our knowledge, no investigations of the pressure behavior of 6H-SrMnO<sub>3</sub> exist, nor has any suggestions of its magnetic structure been made.

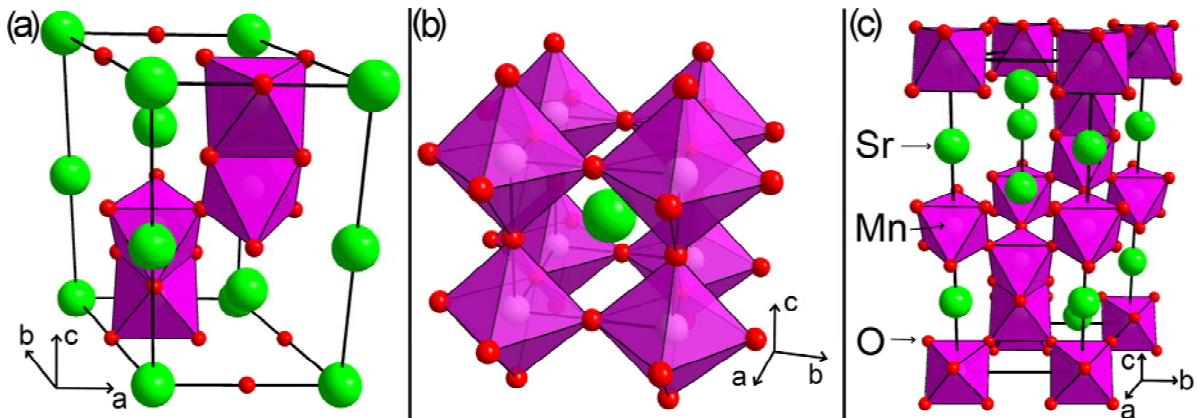


FIG 1. (Color online) (a) 4H-SrMnO<sub>3</sub> unit cell. Alternating corner- and face-sharing is seen along the *c*-axis. (b) 3C-SrMnO<sub>3</sub> unit cell (corners inside octahedra). In this, the perovskite structure, only corner-sharing is observed. (c) 6H-SrMnO<sub>3</sub> unit cell. The degree of corner-sharing has increased from 4H so that each face-sharing dimer is followed by a corner-shared octahedron before being repeated.

The existence of three different polymorphs at room temperature and pressure is quite unique in the perovskite system and the SrMnO<sub>3</sub> system is thus ideal for investigation the effects that structure has on the magnetic and electronic properties in compounds of identical stoichiometry. In the present paper, the room-temperature EoS of 6H-SrMnO<sub>3</sub> to 68 GPa is reported alongside that of 3C-SrMnO<sub>3-x</sub> to 43 GPa, for the first time. The room temperature EoS of 4H-SrMnO<sub>3</sub> is also extended to 60 GPa. *In situ* observation of three transformations of SrMnO<sub>3</sub> phases are reported: (1) from the 4H to the 3C phase at  $\sim 7.0$  GPa and 2000 K, (2) from 4H to 6H at  $\sim 5.9$  GPa and 673 K, and (3) from 3C to 6H at  $\sim 6.7$  GPa and 1273 K. The results are compared to DFT calculations for all three phases. The calculations have also been used to suggest a magnetic structure of 6H-SrMnO<sub>3</sub>, to rationalize its Néel temperature, to investigate the effect of oxygen sub-stoichiometry and to evaluate changes of the band gaps of the 4H and 6H phases versus pressure.

## II. EXPERIMENTAL

### A. Synthesis and characterization

Phase pure 4H-SrMnO<sub>3</sub> was synthesized from a stoichiometric mixture of SrCO<sub>3</sub> and MnO<sub>2</sub> by heating a pressed pellet in air at 1273 K for a total of 60 hours with five intermediate grindings and pressings. See Supplemental Material (SM), part 1<sup>15</sup> for PXRD in which no crystalline impurities could be detected.

3C-SrMnO<sub>3</sub> was synthesized by the method of Negas and Roth<sup>13</sup>, using the 4H-SrMnO<sub>3</sub> as the starting material. The 4H-SrMnO<sub>3</sub> pellet was annealed at 1773 K for 8 hours and subsequently rapidly quenched in cold water. The obtained 3C-SrMnO<sub>3-x</sub> was then annealed at 573 K for 4 hours to re-oxidize the sample to SrMnO<sub>3</sub>. Powder X-Ray Diffraction (PXRD) data on the quenched sample was obtained on beamline BL44B2<sup>16</sup> at SPring8,  $\lambda = 0.499818(3)$  Å, while data on the re-oxidized sample as obtained at 13-ID-D<sup>17</sup>, Advanced Photon Source (APS) prior to the measurements in the DACs.

6H-SrMnO<sub>3</sub> was synthesized by the method of Syono *et al.*<sup>9</sup>, using the Large Volume Press (LVP) located at 13-ID-D<sup>18</sup> at the APS. Experiments were carried out using both 4H-SrMnO<sub>3</sub> and 3C-SrMnO<sub>3</sub> as starting material and the syntheses were followed *in situ* by Energy Dispersive X-ray Diffraction (EDXRD).

### B. High pressure diamond anvil experiments

The measurements of equations of state were all carried out at room temperature using membrane driven DACs. The samples were in all cases loaded in a hole in a rhenium gasket with a diameter of approximately 3/5 of the culet size. Culet sizes between 500 and 200  $\mu\text{m}$  were used, while the gaskets were pre-indented to an initial thickness of approximately 40  $\mu\text{m}$ . Neon was used

as the pressure transmitting medium in all experiments and loaded using the COMPRES/GSECARS gas loading system<sup>19</sup> at the APS, while at the European Synchrotron Radiation Facility (ESRF) a Sanchez Technologies GLS1500 gas loading system was used. This soft gas provides near hydrostatic conditions in the pressure ranges explored. Gold was used as an internal diffraction pressure standard and was measured immediately before and after every sample measurement. The refined unit cell parameter of gold was used to determine the pressure using the equation of state reported by Fei *et al.*<sup>20</sup> The pressures before and after were combined with the uncertainties in the pressure measurement, through the propagation of errors, to yield the final estimate and uncertainty for the pressure during each sample measurement.

The mapping of the 6H-SrMnO<sub>3</sub> EoS was carried out at beamline ID27<sup>21</sup> at the ESRF, using monochromatic radiation with a wavelength of  $\lambda = 0.3738(2)$  Å. Mapping of the 4H- and 3C-SrMnO<sub>3</sub> equations of state and laser heating experiments were all carried out at beamline 13-ID-D<sup>17</sup> at the APS, using monochromatic radiation with a wavelength of  $\lambda = 0.3344(18)$  Å. In both locations, the sample to detector distance and wavelength were calibrated using a LaB<sub>6</sub> standard (NIST SRM 660a). The LaB<sub>6</sub> data was also used to create an instrument resolution file (IRF) which was used in all subsequent refinements of the diffraction data. The 2D data obtained from both beam lines were integrated using the FIT2D software<sup>22</sup> and refined using the FullProf program<sup>23</sup>. The 4H to 3C phase transformation was induced using the 13-ID-D CO<sub>2</sub> laser setup<sup>24</sup> and followed by PXRD.

### C. Large volume press experiments

In situ observation of phase transformations from 4H- and 3C- to 6H-SrMnO<sub>3</sub> were carried out in the LVP at Beamline 13-ID-D<sup>18</sup> at the APS. EDXRD was carried out using a Canberra Ge solid-state detector and the white beam from the undulator with a 2 mm taper. The 2 $\theta$  angle of the detector was calibrated using MgO at ambient conditions. The sample was compressed using a split-cylinder Kawai-type apparatus with 25.4 mm second-stage tungsten carbide (WC) anvils (T-25) in a 1000 ton press. Prior to compression, the sample was pressed to a 2 mm diameter and 1.5 mm tall pellet and mounted inside a Bayreuth-style 14/8 cell assembly<sup>25</sup>. The sample was heated by a graphite heater and the temperature was monitored using an internal C-type W-Re thermocouple. The pressure was determined using either MgO<sup>26</sup> or our own SrMnO<sub>3</sub> equations of state as our pressure markers.

### D. Computational details

DFT calculations were performed with the plane wave pseudo potential code Quantum-Espresso<sup>27</sup>. We employed the PBE functional<sup>28</sup> for the exchange and correlation energy and optimized ultrasoft pseudopotentials<sup>29</sup>. Although small-core norm-conserving pseudo potentials are generally preferable for high pressure calculations, here at the largest applied pressure the change of the Mn-O bond length does not exceed 5%. The semicore 3s3p Mn-states and 4s4p Sr-states are included as valence electrons. We used a plane wave cut-off of 45 Ry and 8x8x8 k-points for Brillouin zone sampling. By this setup, total energy differences between the three polymorphs are

converged to within 0.01 meV per formula unit. A Marzari-Vanderbilt cold smearing of 0.005 Ry was used to treat orbital occupancies at the Fermi level.

As it has been suggested that 4H-SrMnO<sub>3</sub> might show a very slight deviation from hexagonal symmetry close to room temperature<sup>30</sup>, Thus, the energy of the suggested orthorhombic cell was calculated and compared to the 4H phase. The results put the total energy of the two phases within 0.1 meV/formula unit, and therefore all calculations have been performed using the 4H symmetry.

The theoretical equations of state were obtained by a series of variable-cell optimizations, during which the ions were allowed to move, and the cell volume was kept constant according to the experimental points. At the end of the optimization, the stress tensor and the isostatic pressure was extracted. Because the PBE functional is known to slightly overestimate the zero pressure, zero temperature volume of the system, an unconstrained optimization was also performed in order to determine the theoretical  $V_0$  for each polymorph.

At low temperature the cubic polymorph shows a G-type antiferromagnetic order and 4H-SrMnO<sub>3</sub> an AF1 magnetic order, in which all Mn ions are antiferromagnetically coupled along the  $c$ -axis<sup>5,30</sup>. In the calculations, upon applying pressure, the magnetic structure was constrained to be the ground state at zero pressure, but magnitude of the magnetic moment was allowed to change as a function of pressure. The total energy of all possible magnetic arrangements of 6H-SrMnO<sub>3</sub> commensurate with the crystallographic cell was also calculated.

### E. Equation of state fits

The unit cell volumes obtained from refinements of the PXRD models and the DFT calculations were fitted using a 3<sup>rd</sup> order Birch-Murnaghan (BM3) EoS, shown as equation 2.

$$P(V) = 3K_0 f_E (1 + 2f_E)^{5/2} [1 + 3/2(K_0' - 4)f_E], \text{ where } f_E = [(V_0/V)^{2/3} - 1]/2 \quad (2)$$

The EosFit v5.2 program<sup>31</sup> was used to perform the least squares fit and extract the EoS parameters, as well as their covariance matrices.

## III. RESULTS AND DISCUSSION

### A. The crystal structures at ambient conditions

Le Bail refinement of PXRD on 4H-SrMnO<sub>3</sub> at ambient conditions yielded the refined lattice parameters  $a = 5.45088(10)$  Å and  $c = 9.0851(3)$  Å, in good agreement with the experimental values found by others<sup>9,13,14,30,32,33</sup>. The refined model can be found in the SM, part 1<sup>15</sup>.

Rietveld refinement of PXRD on 6H-SrMnO<sub>3</sub> at ambient conditions yielded the lattice parameters  $a = 5.4305(2)$  Å and  $c = 13.4034(13)$  Å, in excellent agreement with the reported structure by Belik *et al*<sup>14</sup>. The full Rietveld refined model can be found in the SM, part 2<sup>15</sup>.

Rietveld refinement of PXRD on 3C-SrMnO<sub>3-x</sub> yielded a unit cell parameter at 300 K of  $a = 3.81109(1)$  Å, and a refined oxygen deficiency of  $x = 0.22(2)$ . Rietveld refinement of the re-oxidized 3C-SrMnO<sub>3</sub> at ambient conditions yielded the refined lattice parameter  $a = 3.8090(7)$  Å. Unfortunately, the presence of preferred orientation in the latter dataset precludes unambiguous stoichiometric information to be extracted from this refinement. Both refined models can be found in the SM, parts 3 and 4<sup>15</sup>.

The value of  $a_0$  for the re-oxidized sample is not in perfect agreement with others<sup>13,14,34</sup> indicating that complete re-oxidization might not have been achieved. This is noteworthy as the  $a_0$  obtained from this measurement lies outside the trend of the full EoS mapping of the 3C-phase, which used a fraction of the same sample. This data point has therefore not been used in the fitting of the 3C EoS. Because of the possibility that the experimental 3C-SrMnO<sub>3</sub> sample was not fully re-oxidized, it will be referred to as 3C-SrMnO<sub>3- $\delta$</sub>  for the rest of the paper. The effect of sub-stoichiometry on the oxygen position is discussed in detail in section III.D

## B. Equation of state measurements

The results of the DAC experiments on 4H-SrMnO<sub>3</sub>, 6H-SrMnO<sub>3</sub> and 3C-SrMnO<sub>3- $\delta$</sub>  are reported in Fig. 2. Also plotted is a BM3 EoS fit to the obtained data as well as the results of the DFT calculations.

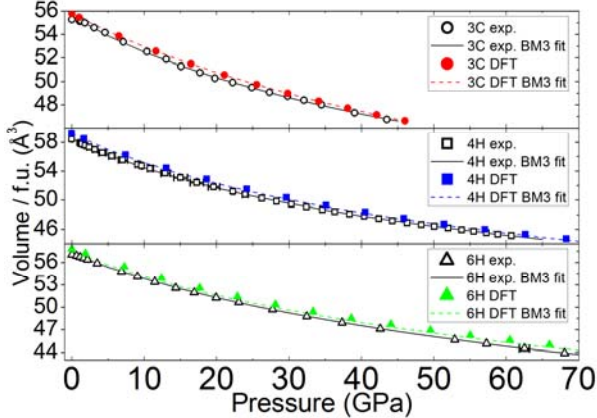


FIG. 2. (Color online) Open symbols: The observed unit cell volumes of 3C-, 4H- and 6H-SrMnO<sub>3</sub> as a function of pressure at room temperature. When not plotted, error bars are smaller than the symbols. Closed symbols: As open, but from DFT. Solid lines: 3<sup>rd</sup> order Birch-Murnaghan (BM3) equation of state fits to each data set. Dashed lines: As solid lines, but fitted to the DFT results.

The values of  $V_0$ ,  $K_0$  and  $K_0'$  for 4H-SrMnO<sub>3</sub> extracted from the BM3 fit are listed in Table 1 along with the results from previous studies by others. The equivalent data for 6H-SrMnO<sub>3</sub> and 3C-SrMnO<sub>3- $\delta$</sub>  are listed in Tables 2 and 3. The DFT values for  $V_0$ ,  $K_0$  and  $K_0'$  were obtained by fitting a BM3 EoS to the DFT results.

TABLE I. Values of the zero pressure volume, bulk modulus and its first pressure derivative for 4H-SrMnO<sub>3</sub> from this study and other reports.

	$V_0$ (Å <sup>3</sup> )	$K_0$ (GPa)	$K_0'$	Pressure medium
Present study:				
4H BM3	233.86(2)	115.6(11)	5.44(8)	Neon
4H DFT BM3	237.8(5)	117(3)	4.98(13)	
PXRD $V_0$	233.774(11)			
Earlier reported experiments:				
Syono <i>et al.</i> <sup>9</sup>	233.6(1)			
Negas & Roth <sup>13</sup>	233.429			
Battle <i>et al.</i> <sup>32</sup>	232.754(17)			
Søndenå <i>et al.</i> <sup>5</sup>	Not reported	136	4.16	Nitrogen
Liu <i>et al.</i> <sup>35</sup>	232.9(1)	266(4)	4 (fixed)	4:1 methanol:ethanol
Earlier reported calculations:				
Søndenå <i>et al.</i> <sup>5</sup>	237.808	126	4.40	

TABLE II. Values of the zero pressure volume, bulk modulus and its first pressure derivative for 6H-SrMnO<sub>3</sub> from this study and other reports.

	$V_0$ (Å <sup>3</sup> )	$K_0$ (GPa)	$K_0'$	Pressure medium
Present study:				
6H BM3	343.09(14)	143.7(17)	4.40(10)	Neon
6H DFT BM3	347.99(19)	140.0(13)	4.86(5)	
PXRD $V_0$	342.31(21)			
Earlier reported experiments:				
Syono <i>et al.</i> <sup>9</sup>	342.3(3)			
Belik <i>et al.</i> <sup>14</sup>	342.0929(3)			

TABLE III. Values of the zero pressure volume, bulk modulus and its first pressure derivative for 3C-SrMnO<sub>3</sub> from this study and other reports.

	$V_0$ (Å <sup>3</sup> )	$K_0$ (GPa)	$K_0'$	Pressure medium
Present study:				
3C-SrMnO <sub>3-δ</sub> BM3	55.58(2)	146(5)	6.4(5)	Neon
3C DFT BM3	55.765(7)	172.5(4)	4.413(18)	
PXRD $V_0$	55.259(3)			
Earlier reported experiments:				
Negas & Roth <sup>13</sup>	55.132			
Takeda & Ōhara <sup>36</sup>	54.9			
Chmaissem <i>et al.</i> <sup>34</sup>	55.1065(1)			
Earlier reported calculations:				
Fuks <i>et al.</i> <sup>37</sup>	56.845	118.7		
Søndenå <i>et al.</i> <sup>5</sup>	55.918	166	4.70	

When fitting PV data, the values of  $K_0$  and  $K_0'$  always correlate heavily, which means that merely reporting their final values and their assumed independent uncertainties (as in the tables) is

somewhat misleading. To better illustrate the range of values that are equally likely, a plot of the  $3\sigma$  confidence ellipse in  $K_0$  vs  $K_0'$  is utilized in Fig. 3. Solid lines show experimental results and dashed lines show theoretical results.

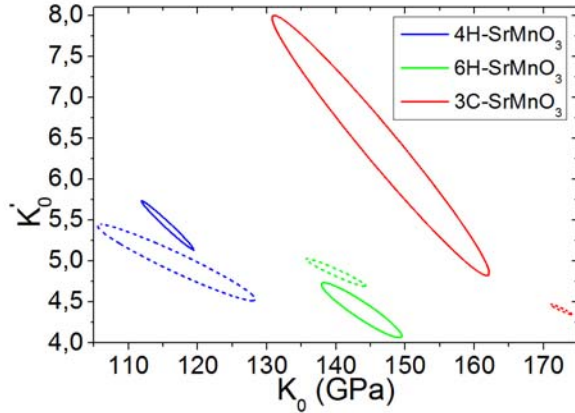


FIG. 3. (Color online) Plot of the correlated values of  $K_0$  and  $K_0'$  to 3 standard deviations, when taking their covariance into account. Solid lines are experimental results, dashed lines are DFT results.

As can be seen in Fig. 2, DFT systematically overestimates the volume compared to experiment for any given pressure. However, the agreement within a 1-2% is considered quite satisfactory for perovskite structures<sup>38</sup>. The values of  $V_0$  for 4H- and 6H-SrMnO<sub>3</sub> polymorphs fit quite well with all previous experimental reports, while  $V_0$  of 3C-SrMnO<sub>3</sub> shows the largest deviation from other findings.

The experimental results for 3C-SrMnO<sub>3- $\delta$</sub>  are the least certain and also show the largest difference when compared to theory. The values of  $K_0$  and  $K_0'$  correlate with  $V_0$ , the value of which is probably too large, an effect induced by the oxygen content of the sample being slightly below 3.00. The effect of oxygen sub-stoichiometry is discussed further in section III.D. The fact that the PV relation was not measured for 3C-SrMnO<sub>3- $\delta$</sub>  to pressures as high as for the 4H and 6H polymorphs also plays a role. 3C-SrMnO<sub>3</sub> is expected to be significantly harder than both hexagonal phases as this phase is induced by pressure. This is also what DFT predicts for the 3C-SrMnO<sub>3</sub> phase and the cause of the discrepancy is discussed further in section III.D.

The bulk modulus of 4H-SrMnO<sub>3</sub> determined here and its pressure derivative are significantly different from all previous reports, especially that of Liu *et al.*<sup>35</sup> The values for 6H and 3C-SrMnO<sub>3</sub> are the first ones reported experimentally.

The first thing to note, when comparing the present results to those from others, is the choice of formalism for the utilized equation of state. Values of the bulk modulus and its pressure derivative obtained from different equations of state are generally not comparable at high compressions<sup>31</sup>. This study utilizes the 3<sup>rd</sup> order Birch-Murnaghan equation of state as the compression ratio,  $V/V_0$ , is smaller than 0.9, below which the simpler Murnaghan equation of state

(used in Søndena *et al.* and Liu *et al.*) is no longer applicable. The simpler Murnaghan EoS is shown as equation 3.

$$P(V) = K_0 / K_0' \left[ (V/V_0)^{K_0'} - 1 \right] \quad (3)$$

When using the Murnaghan EoS on the presented data (merely for comparison as the fit is inadequate), the values for 4H-SrMnO<sub>3</sub> of  $K_0 = 119(1)$  GPa,  $K_0' = 4.76(6)$  are obtained, still significantly different from both previous studies. Likewise, the values  $K_0 = 151(4)$ ,  $K_0' = 5.6(3)$  are obtained for 3C-SrMnO<sub>3-δ</sub> using the same approach.

The different pressure media used across the studies also play an important role. This study used neon which only shows 1% deviation from hydrostatic conditions at 50 GPa<sup>39</sup>, while Søndena *et al.* used nitrogen (hydrostatic to 10 GPa<sup>39</sup>) and Liu *et al.* used 4:1 methanol:ethanol (hydrostatic to 10.5 GPa<sup>39</sup>). It is worth noting that the calculated results of Søndena *et al.* are in better agreement with the present data than their experimental findings. This makes sense as DFT does not take the pressure medium into account and neon behaves closer to the hydrostatic conditions that DFT assumes. Furthermore, Liu *et al.* reported unsatisfactory placement of the ruby in the DAC experiment which will also contribute to the difference between their results and those presented here.

Lastly it is worth mentioning that the 4H-phase displays anisotropic compression from 0 to roughly 30 GPa, with the *c*-axis being slightly more compressible. Above 30 GPa compression of the cell is isotropic, keeping the *a/c* ratio constant. See the SM, part 5<sup>15</sup>, for a plot of *a/c* vs *P*. A similar trend was not observed in the relaxed cells of the DFT calculations.

## C. In situ observation of phase transformations

### 1. 4H- to 3C-SrMnO<sub>3</sub>

In an attempt to determine the transition pressure of the transformation of 4H to 3C-SrMnO<sub>3</sub>, laser heating of a 4H-SrMnO<sub>3</sub> sample was carried out at 6.975(12) GPa (before heating, not measured after) in a DAC. A Le Bail refinement of PXRD on the 4H sample before heating can be seen in Fig. 4(a). It yields the 4H lattice parameters  $a = 5.3577(3)$  Å,  $c = 8.9551(8)$  Å.

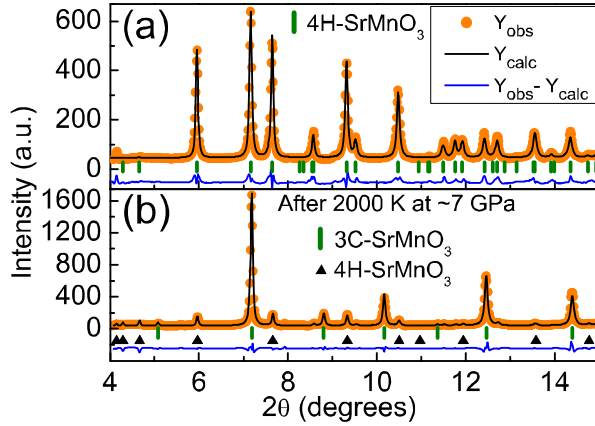


FIG. 4. (Color online) (a) PXRd data and Le Bail refinement of 4H-SrMnO<sub>3</sub> in the DAC data at room temperature, before heating. (b) PXRd data and Le Bail refinement of the same sample after heating. The sample has clearly transformed to 3C-SrMnO<sub>3</sub>, though traces of 4H remain. Background has been subtracted from both plots.

At this pressure, the sample was heated to  $2000 \pm 100$  K, held at this temperature for 15 minutes after which it was quenched to room temperature. A Le Bail refinement of PXRd on the sample after quenching is shown in Fig. 4(b). It yields the 3C lattice parameter  $a = 3.7761(1)$  Å. A clear transformation from 4H to 3C-SrMnO<sub>3</sub> can be seen. The sample still contains a few percent 4H-SrMnO<sub>3</sub> after heating, while no trace of 6H-SrMnO<sub>3</sub> is visible.

In another DAC experiment a 4H sample was compressed to 6.465(16) GPa (before heating, not measured after) and then subjected it to  $2300 \pm 200$  K. A phase transition to a cubic phase was also observed in this case. However, the cubic unit cell parameter found by a Le Bail refinement at this pressure,  $a = 3.8411(1)$  Å, was significantly larger than that found at zero pressure for the 3C-SrMnO<sub>3- $\delta$</sub>  sample, where  $a = 3.80891(6)$  Å.

In their study of 4H- and 3C-SrMnO<sub>3</sub>, Søndena *et al.* predicted that the cubic polymorph should be stable at volumes less than approx.  $53$  Å<sup>3</sup> per formula unit. In their paper, they calculated that this volume should correspond to 12 GPa. Note that this transition pressure ignores the existence of the 6H polymorph, which was synthesized by Belik *et al.* at 6 GPa and also does not consider temperature. As will be shown in section III.D, the 6H phase is predicted to be stable at this pressure at zero Kelvin. This indicates that entropy differences between the three phases must play an important role in the stabilization of the 3C phase at this lower pressure and higher temperature.

The observation of a cubic phase with  $a > a_0$  is accounted for when it is noticed that the ambient unit cell of 3C-SrMnO<sub>2.78</sub> is larger than that of 3C-SrMnO<sub>3- $\delta$</sub> . It is concluded that the sample was reduced inside the DAC as a result of the high temperature. Indeed, it is this high temperature reduction which was observed at ambient pressure and 1773 K by Negas & Roth and which was used to synthesize 3C-SrMnO<sub>3</sub> in the first place<sup>13</sup>. It is also possible that the inert neon

pressure medium has an effect. That the onset of reduction moves to higher temperature (i.e. the equilibrium is shifted towards to solid phase) when the sample is subjected to high pressure is as expected when reduction involves the evolution of free oxygen.

## 2. 4H- to 6H-SrMnO<sub>3</sub>

The first *in situ* observation of the formation of 6H-SrMnO<sub>3</sub> from 4H-SrMnO<sub>3</sub> was carried out by performing EDXRD in the Large Volume Press (LVP) at 13-ID-D at the APS. In this experiment the load was increased to produce a pressure of 5.9 GPa. A Le Bail refinement of EDXRD on the unheated sample can be seen in Fig. 5(a). It yields the 4H lattice parameters  $a = 5.4099(6)$  Å,  $c = 9.059(1)$  Å. Two regions where W fluorescence was seen are masked out (59 and 67 keV).

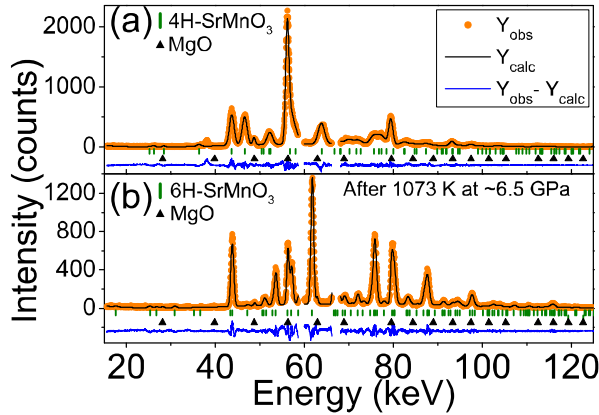


FIG. 5. (Color online) (a) EDXRD and Le Bail refinement of 4H-SrMnO<sub>3</sub> inside the LVP assembly at 5.91(2) GPa before heating. Top markers are 4H-SrMnO<sub>3</sub> peaks while bottom markers are MgO. (b) EDXRD and Le Bail refinement of 6H-SrMnO<sub>3</sub> inside the LVP at room temperature after heating. Top markers are 6H-SrMnO<sub>3</sub> while the bottom markers are MgO.

While keeping the load constant, the temperature was slowly increased to 673 K where the first changes in peak intensities were observed. This temperature was kept for 16 min after which the heating was turned off and the sample cooled to room temperature over the course of 5 minutes. As traces of 4H-SrMnO<sub>3</sub> were still visible, additional heating was carried out at 1073 K for 5 min, then pressure was increased to approximately 6.5 GPa and the sample re-annealed at 1073 K for 5 minutes. A Le Bail refinement of EDXRD on the sample after all heating is seen in Fig. 5(b). It yields the 6H lattice parameters  $a = 5.3524(2)$  Å,  $c = 13.313(1)$  Å.

After pressure was released, the sample was recovered as a solid pellet which was subsequently crushed to a fine powder and measured using angular PXRD prior to mapping of the 6H EoS in a DAC. The result of this measurement was reported in section III.A.

After the final heating at 6.5 GPa and 1073 K no trace of 4H-SrMnO<sub>3</sub> was observed, i.e. complete transformation was observed (Fig. 5(b)). The unit cell parameters of 6H-SrMnO<sub>3</sub> at ambient conditions are in excellent agreement with Belik *et al.*<sup>14</sup>

### 3. 3C- to 6H-SrMnO<sub>3</sub>

An attempt was made at synthesizing 6H-SrMnO<sub>3</sub> from the 3C phase in the LVP. The sample was compressed to 6.7 GPa at room temperature before heating. A Le Bail refinement of EDXRD on the unheated sample can be seen in Fig. 6(a). It yields the 3C lattice parameter  $a = 3.7656(3)$  Å. While keeping the load constant, the temperature was ramped to 1273 K at a rate of 50 K/min and held at this temperature for 50 min. The temperature was then reduced to room temperature over 17 min. A Le Bail refinement of EDXRD on the sample after annealing is seen in Fig. 6(b). It yields the 6H lattice parameters  $a = 5.3979(3)$  Å,  $c = 13.357(2)$  Å.

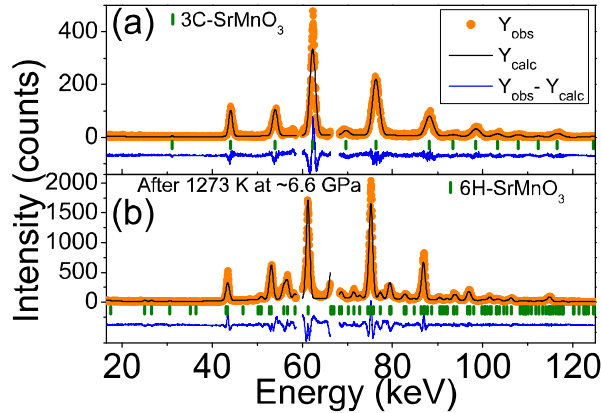


FIG. 6. (Color online) (a) EDXRD and Le Bail refinement of 3C-SrMnO<sub>3</sub> inside the LVP assembly at room temperature and 6.66 GPa before heating. (b) EDXRD and Le Bail refinement of 6H-SrMnO<sub>3</sub> inside the LVP assembly at room temperature. Notice the weaker, but clearly significant, peaks between the strong reflections that were also present in the starting 3C-SrMnO<sub>3</sub>.

The phase in Fig. 6(b) is obviously different from the starting 3C-SrMnO<sub>3</sub> seen in Fig. 6(a), since a number of weaker peaks have appeared between the strong positions present in the cubic phase; e.g. reflections (207), (215) and (303) at 79.5 keV which are extinct in the cubic phase. The 6H-SrMnO<sub>3</sub> model, which incorporates these new peaks, is thus clearly superior and we conclude that a phase transformation from the 3C to 6H phase has taken place. The 6H phase is thus not merely a metastable phase resulting from a quench to ambient conditions, but is the thermodynamically stable phase at these PT conditions.

## D. Computational investigations of SrMnO<sub>3</sub>

### 1. The relative stability of the three phases

In order to compare the experimental observations of phase transformations with theory, total energy calculations of relaxed unit cells were performed. At each volume, the unit cell shape and atomic positions were allowed to relax freely in order to minimize the energy. The volume ranges cover all experimental pressures explored in this study. No volumes larger than that which corresponds to  $P_{\text{DFT}} = 0$  were explored, as they are physically meaningless. A plot of the resulting relative energies can be seen in Fig. 7. At zero pressure, the total internal energy of the 6H phase is 44.9 meV/f.u. higher than 4H while the 3C phase is 0.23402 eV/f.u. above 4H.

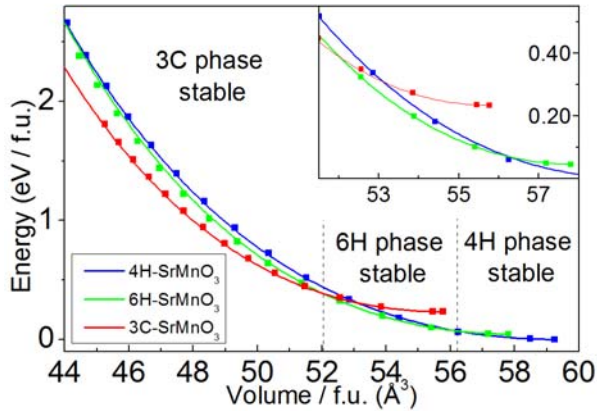


FIG. 7. (Color online) The total internal energies (relative to the 4H phase at zero pressure equilibrium volume) of the three SrMnO<sub>3</sub> phases as a function of volume per formula unit. The largest volume for each phase corresponds to that at  $P_{\text{DFT}} = 0$ . Points are DFT results while the full lines represent the BM3 fits to the DFT  $P(V)$  data combined with  $E_0$  from DFT. Inset shows a zoom around the 6H stability region for clarity, with the same axis units.

Phase transition pressures were found from the common tangents of each pair of curves. Along this slope, the enthalpies of the two phases are equal (as the temperature in the calculations is 0 K). The slopes of these tangents are found to be 5.9(3) GPa for the 4H to 6H transition and 18.1(2) GPa for the 6H to 3C transition. Full tables of volumes, total internal energies and pressures can be found in the SM, part 6<sup>15</sup>.

The results clearly show 4H to be stable at large volumes, 6H to be favored in an intermediate range and 3C to be stable at high compressions. For comparison, if only the 4H and 3C phases are considered the equilibrium pressure is 13.5(5) GPa, somewhat higher but in fair agreement with the 12 GPa reported by Søndena *et al.*<sup>5</sup>

## 2. Possible effects of oxygen sub-stoichiometry

The 3C phase of SrMnO<sub>3</sub> is synthesized through an oxygen sub-stoichiometric intermediate product which is subsequently re-oxidized. Therefore, the possibility exists that the 3C sample is not truly of full SrMnO<sub>3</sub> stoichiometry, but is instead SrMnO<sub>3- $\delta$</sub> , where  $y$  could fall in the range of  $0 < y < 0.25$ . The effect of such sub-stoichiometry has been explored experimentally for several lanthanoid manganates<sup>40</sup> doped with Sr, and also for 4H-SrMnO<sub>3</sub><sup>13</sup>, but no calculations of the total energy has been carried out for sub-stoichiometric SrMnO<sub>3- $\delta$</sub>  thus far. In the study on the lanthanoid

manganates, the result of reducing  $\text{Mn}^{4+}$  to  $\text{Mn}^{3+}$  was a lowering of the tolerance factor and an increase in volume. From tolerance factor point of view, this should result in a stabilization of the corner-sharing polymorph, i.e. the cubic phase should be stabilized with respect to the 4H and 6H phases. However, these rules are entirely empirical and proper DFT calculations have to be carried out in order to get a thermodynamic understanding of the behavior of sub-stoichiometric compounds under pressure.

To simulate the high pressure behavior of  $\text{SrMnO}_{3-\delta}$ , two random oxygen ions (not belonging to the same  $\text{SrO}_6$  octahedron) were removed from a 4H unit cell. This results in the stoichiometry  $\text{SrMnO}_{2.5}$ , enhancing the possible effects of oxygen sub-stoichiometry. This cell was then fully relaxed within DFT (coordinates and relative cell vectors) at a fixed volume. The total energy, isostatic pressure and resulting enthalpy were then extracted from the relaxed cell. For the 3C phase, a  $2 \times 1 \times 1$  super cell was constructed and an oxygen atom was removed before performing the same type of relaxation and extraction of energy, pressure and enthalpy. The results of these calculations can be seen in Fig. 8 where the enthalpy difference between the 4H and 3C structures at the stoichiometry  $\text{SrMnO}_{2.5}$  and  $\text{SrMnO}_3$  are plotted as a function of pressure. Full tables of cell volumes, pressure and energies can be found in the SM, part 7<sup>15</sup>.

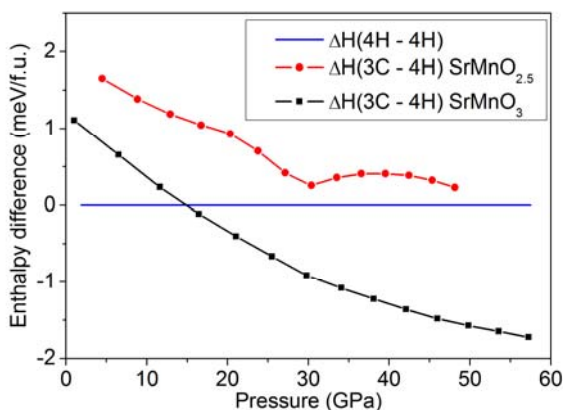


Fig.8 (Color online) Enthalpy difference per formula unit of the 4H and 3C structures of  $\text{SrMnO}_{2.5}$  and  $\text{SrMnO}_3$  as a function of pressure. Points show DFT results and lines are a guide to the eye. As  $\text{SrMnO}_3$  loses oxygen, the black line will move towards the red.

The effect of removing oxygen from the 4H and 3C unit cells of  $\text{SrMnO}_3$  is quite large. Where in the stoichiometric compound, 3C becomes more stable than 4H at 13.5 GPa (see Fig. 7 in the previous section), once the compound reaches the stoichiometry  $\text{SrMnO}_{2.5}$ , the 4H structure is more stable at zero kelvin at all investigated pressures.

The DFT BM3 EoS of the 3C phase also changes quite drastically, with  $K_0$  decreasing to 121 GPa in  $\text{SrMnO}_{2.5}$  from 172 GPa in  $\text{SrMnO}_3$ . It is worth noting that the experimental value of 142 GPa obtained in this study is closer to the theoretical  $K_0$  from  $\text{SrMnO}_{2.5}$  than that of  $\text{SrMnO}_3$ . The  $V_0$ 's resulting from ambient PXRD on 3C- $\text{SrMnO}_{3-\delta}$  and the BM3 fit of the experimental data are in both cases larger than those reported by others, which also suggests that the 3C sample

measured was in fact slightly reduced. However, while one might be tempted to deduce the value of  $y$  in  $\text{SrMnO}_{3-\delta}$  from a direct interpolation of the change in  $K_0$ , this is not advisable as reduction also affects the zero pressure volume,  $V_0$ , which in turn correlates heavily with  $K_0$ . A better option might be to perform a linear interpolation on the unit cell parameter  $a$  in the re-oxidized cell. This would lead to an estimated value of  $y$  of about 0.1.

The effect of reducing  $\text{SrMnO}_3$  is thus likely to have affected our results in two ways by: 1) Destabilizing the 3C phase relative to the 4H phase thus suppressing the possible transition of the latter to the former at high pressure and low temperatures and 2) reducing the bulk modulus of the 3C phase by quite a significant amount.

Furthermore, as the enthalpy of  $3\text{C-SrMnO}_{2.5}$  is higher than that of  $4\text{H-SrMnO}_3$ , it must be concluded that the transition observed by Negas & Roth<sup>13</sup> from  $4\text{H-SrMnO}_{3-x}$  to  $3\text{C-SrMnO}_{3-x}$  at atmospheric (“zero”) pressure is driven by changes in entropy.

### 3. *Magnetic structure and band gap of 6H-SrMnO<sub>3</sub>*

To date, no suggestion for the magnetic structure of  $6\text{H-SrMnO}_3$  has yet been published. Through magnetic susceptibility measurements, Belik *et al*<sup>14</sup>. found the phase to be antiferromagnetic, with  $T_N = 235$  K, slightly lower than that of  $3\text{C-SrMnO}_3$  ( $T_N = 240$  K) and somewhat lower than  $4\text{H-SrMnO}_3$ ,  $T_N = 280$  K.

The energies of all 32 possible spin states in the unit cell have been calculated and an antiferromagnetic ground state very similar to the AF1 structure in  $4\text{H-SrMnO}_3$  has been found<sup>30</sup>. Since the internal stress tensor did not change appreciably for low-lying spin excitations, it is concluded that the magneto-elastic coupling is negligible in this system and thus it has not been included in the calculations. No magnetic super cells were sampled. The calculated magnetic moments on Mn are  $2.22 \mu_B$  for Mn1 and  $2.26 \mu_B$  for Mn2 at zero pressure. Mn1 is in the corner-sharing octahedra, Mn2 is inside the face-sharing octahedra. The magnetic moment is calculated by integrating the spin density inside a muffin-tin sphere of radius  $0.77 \text{ \AA}$ . Full tables and figures of the explored magnetic configurations and their respective energies can be found in the SM, part 8<sup>15</sup>.

The antiferromagnetic coupling of each Mn-Mn pair along  $c$  is the most favored structure. It is plotted as AF1 in Fig. 9(a). The first magnetic excitation corresponds to a ferromagnetic coupling of the Mn ions at the center of face-sharing octahedra. It is plotted as AF2 in Fig. 9(b). The excitation costs  $24.5 \text{ meV}$  per formula unit, which is close to the thermal energy at room temperature.

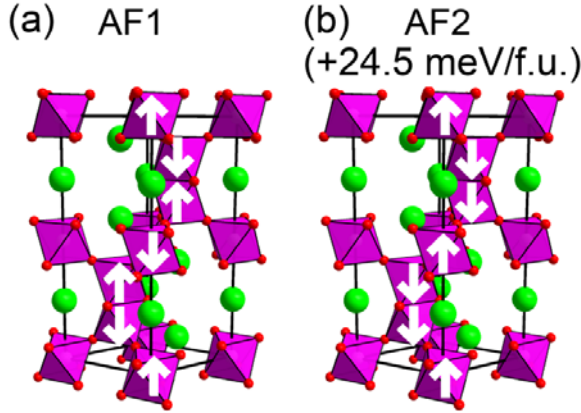


FIG. 9. (Color online) (a) Suggested antiferromagnetic structure of 6H-SrMnO<sub>3</sub>. (b) The first magnetic excitation found through DFT at 24.5 meV/f.u. above the ground state configuration.

In 4H-SrMnO<sub>3</sub>, the first magnetic excitation found by Søndena *et al.*<sup>5</sup> is 23 meV/f.u. unit above the ground state, while in 3C-SrMnO<sub>3</sub> they found it to be 25 meV/f.u. above the ground state. The first magnetic excitation in 6H-SrMnO<sub>3</sub> is thus of very similar energy to the other existing polymorphs. Søndena *et al.*<sup>5</sup> calculated 2.47  $\mu_B$  per Mn in both the 4H and 3C phases, somewhat larger than the magnetic moments found for the 6H phase.

By calculating the susceptibility as a function of temperature from the Boltzmann distribution of the energies of the 32 spin configurations (6 sites), a crude approximation for the Néel temperature can be found. This is done in the SM, part 8<sup>15</sup>, yielding a broad peak at about 190 K. This is in fairly good agreement with the experimental value of 235 K due to the broadening by the finite size of the system and the nature of the approximation.

As the DFT calculation of the possible magnetic structures and their energies assumed collinear spins and neglected spin-orbit coupling, non-collinear spin calculations were also performed, with a denser mesh of k-points. The magnetic anisotropy energy was estimated to be in the order of 0.1 meV per unit cell, resulting in a very slight preference for spin alignment along the *c*-axis.

Finally, the band gap has been estimated as a function of pressure for the 6H and 4H phases, while the 3C phase is metallic within DFT. The 6H gap starts out at about 1.3 eV at zero pressure, before increasing to a maximum value of about 1.5 eV at 50 GPa after which it decreases. Belik *et al.*<sup>14</sup> measured the resistivity versus temperature of 6H-SrMnO<sub>3</sub> and used this to estimate a transport gap of 0.24 eV. This value cannot be directly compared to the one from DFT, as it is a measure of the barrier for electron transport and as such does not represent the DFT band gap. The 4H gap starts at about 1.8 eV in our calculations and decreases monotonically with pressure. The initial

value is similar to the 1.60 eV obtained by DFT by Søndena *et al.*<sup>5</sup> Plots of band gaps versus both volume and pressure are shown in the SM, part 9<sup>15</sup>.

### E. Towards a PT phase diagram

As a result of the above observations, a visual representation of the present knowledge of the phase behavior of SrMnO<sub>3</sub> as a function of pressure and temperature is outlined in Figure 10. This diagram is made by combining the reported synthesis conditions of the 6H phase (points in the 6H stability region), the room pressure investigations performed previously by others (points at “zero” pressure) and the present experimental and DFT results (points at zero K). A large PT region results where the 6H phase should be stable. Very high temperatures (above 1800 K) seem to stabilize the 3C phase. If the pressure is too low at these temperatures, the compound loses oxygen whilst maintaining the cubic structure. This thus introduces an important third dimension to the diagram, namely the value of  $x$  in SrMnO<sub>3-x</sub>. Experiments carried out inside these regions (graded and marked with the corresponding phase name in Fig. 10) or on samples obtained from this region should pay careful attention to whether partial reduction has taken place.

The effect of reduction on the relative stabilities of the three phases is hinted at in Fig. 8, where partial reduction seems to stabilize the face-sharing phase over the corner-sharing one. This would serve to move the stability border of 4H upwards in pressure as one moves along the axis of  $x$  in SrMnO<sub>3-x</sub>. At high temperatures, the entropy of the 3C structure must be greater than that of the 4H structure, evidenced by the fact that the 3C structure was observed in the experiments of Negas & Roth<sup>13</sup> for the stoichiometry  $x > 0.279$ . Further calculations would have to be performed in order to establish whether the 6H stability field is expanded or contracted by movement along the third dimension.

At sufficiently high pressures, the stoichiometric 3C phase should be stable with respect to the two hexagonally distorted polymorphs. From the diagram it is clear that future studies should be conducted in the PT region of 10-20 GPa and 400-1600 K in order to experimentally establish the upper border between 3C and 6H-SrMnO<sub>3</sub>.

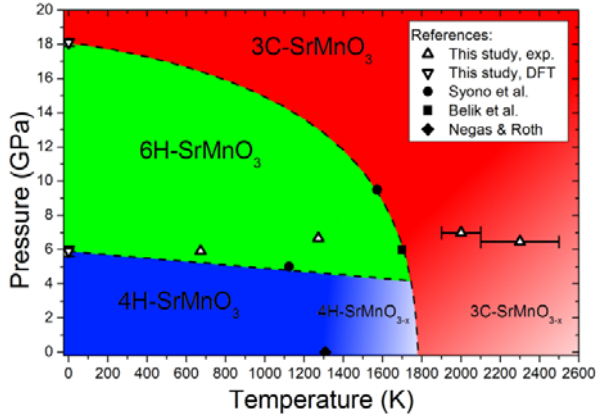


FIG. 10. (Color online) Pressure / temperature plot summarizing the present knowledge of phase behavior of  $\text{SrMnO}_3$ . P and T error bars are not shown when smaller than symbols. The point on the stability border at room pressure indicates the temperature where transformation into the right hand phase was observed. Points at zero K represent DFT predictions of where the two adjacent phases have equal enthalpy. All other points indicate synthesis conditions at which transformation into the phase has been observed. Shaded regions indicate areas where reduction of  $\text{SrMnO}_3$  seems unavoidable. It is emphasized that the exact location of the borders are still quite uncertain, especially in the regions far from experimental points.

#### IV. CONCLUSION

A comprehensive study of the phase relations in the  $\text{SrMnO}_3$  system under high pressure and high temperature conditions has been performed, using both experimental observations and DFT calculations. The compound goes through two phase transitions as pressure is increased, from the hexagonally distorted 4H polymorph, over the less distorted 6H polymorph to the ideal cubic 3C perovskite structure at high pressure and temperatures. Excessive heating results in the loss of oxygen from the compound, even at high pressures. This reduction strongly affects the thermodynamics of the compound and seems to favor face-sharing over corner-sharing at low temperatures, while at high temperatures the entropy of the 3C phase overcomes the enthalpy barrier against transformation, resulting in the corner-sharing polymorph.

A magnetic structure for the 6H polymorph is proposed along with a simple model for comparing the predicted Néel temperature with the experimental one. The magnetic structure is similar to the one found for the 4H polymorph.

While Fig. 10 gives a broad outline of the phases which should be observed at thermodynamic equilibrium in this system (and highlights areas where knowledge is still lacking), severe kinetic barriers still exist and phase transformations are not observed at room temperature. This has the advantage that the EoS for 4H- $\text{SrMnO}_3$  could be determined to 61 GPa and the EoS for 6H- $\text{SrMnO}_3$  to 68 GPa without observing transitions. Furthermore, reduction of the compound happens easily in the shaded regions of the figure and one should thus perform experiments while paying great attention to the oxygen stoichiometry in these regions.

## ACKNOWLEDGEMENTS

The majority of the studies were performed at GeoSoilEnviroCARS (Sector 13), Advanced Photon Source (APS), Argonne National Laboratory. GeoSoilEnviroCARS is supported by the National Science Foundation – Earth Sciences (EAR-1128799) and Department of Energy – GeoSciences (De-FG02-94ER14466). Use of the Advanced Photon Source was supported by the U. S. Department of Energy, Office of Science, Office of Basic Energy Sciences, under contract No. DE-AC02-06CH11357. Use of the COMPRES-GSECARS gas loading system was supported by COMPRES under NSF Cooperative Agreement EAR 11-57758 and by GSECARS through NSF grant EAR-1128799 and DOE grant DE-FG02-94ER14466. The ID27 beamline staff at ESRF is gratefully acknowledged for access to beamtime. The RIKEN-Harima Institute is gratefully acknowledged for beamtime at BL44B2 at the Spring8 synchrotron facility. DanScatt is thanked for financial support for travel expenses for beamtimes. MB thanks the Villum Foundation and CMC for funding. CMC is a Center of Excellence funded by the Danish National Research Foundation (DNRF93). We would also like to thank the reviewers for their comments which have served to greatly improve the quality of the manuscript.

- 
- [1] T. Takenaka, K. Maruyama, and K. Sakata, *Jpn. J. Appl. Phys.* **1** **30**, 2236 (1991).  
[2] M. V. Raymond and D. M. Smyth, *J. Phys. Chem. Solids* **57**, 1507 (1996).  
[3] J. B. Goodenough, *Phys. Rev.* **100**, 564 (1955).  
[4] M. A. Pena and J. L. G. Fierro, *Chem. Rev.* **101**, 1981 (2001).  
[5] R. Søndenå, P. Ravindran, S. Stølen, T. Grande, and M. Hanfland, *Phys. Rev. B.* **74**, 144102 (2006).  
[6] M. Imada, A. Fujimori, and Y. Tokura, *Rev. Mod. Phys.* **70**, 1039 (1998).  
[7] V. M. Goldschmidt, *Naturwissenschaften* **14**, 477 (1926).  
[8] Y. Inaguma, M. Yoshida, T. Tsuchiya, A. Aimi, K. Tanaka, T. Katsumata, and D. Mori, *J. Phys.: Conf. Ser.* **215**, 12131 (2010).  
[9] Y. Syono, S. I. Akimoto, and K. Kohn, *J. Phys. Soc. Jpn.* **26**, 993 (1969).  
[10] M. Murakami, K. Hirose, K. Kawamura, N. Sata, and Y. Ohishi, *Science* **304**, 855 (2004); A. R. Oganov and S. Ono, *Nature* **430**, 445 (2004).  
[11] M. W. Lufaso and P. M. Woodward, *Acta Crystallogr. Sect. B* **57**, 725 (2001).  
[12] R. D. Shannon, *Acta Crystallogr. Sect. A* **32**, 751 (1976).  
[13] T. Negas and R. S. Roth, *J. Solid State Chem.* **1**, 409 (1970).  
[14] A. A. Belik, Y. Matsushita, Y. Katsuya, M. Tanaka, T. Kolodiaznyi, M. Isobe, and E. Takayama-Muromachi, *Phys. Rev. B* **84**, 094438 (2011).  
[15] See Supplemental Material at [\[URL will be inserted by publisher\]](#) for ambient conditions PXRD of 4H-, 6H- and 3C-SrMnO<sub>3-x</sub> and re-oxidized 3C-SrMnO<sub>3</sub>, 4H *a/c* ratio vs pressure, the possible commensurate magnetic structures of 6H-SrMnO<sub>3</sub> along with their energies and estimate of the Néel temperature, the effect of oxygen vacancies on the total energy of the 4H and 3C phases and the evolution of the band gap of the 4H and 6H phases versus pressure.  
[16] S. Adachi, T. Oguchi, H. Tanida, S. Y. Park, H. Shimizu, H. Miyatake, N. Kamiya, Y. Shiro, Y. Inoue, T. Ueki, and T. Iizuka, *Nucl. Instrum. Methods* **467**, 711 (2001).

- [17] G. Y. Shen, V. B. Prakapenka, P. J. Eng, M. L. Rivers, and S. R. Sutton, *J. Synchrotron Radiat.* **12**, 642 (2005).
- [18] Y. B. Wang, M. Rivers, S. Sutton, N. Nishiyama, T. Uchida, and T. Sanehira, *Phys. Earth Planet In.* **174**, 270 (2009).
- [19] M. Rivers, V. B. Prakapenka, A. Kubo, C. Pullins, C. M. Holl, and S. D. Jacobsen, *High Pressure Res.* **28**, 273 (2008).
- [20] Y. W. Fei, A. Ricolleau, M. Frank, K. Mibe, G. Y. Shen, and V. Prakapenka, *Proc. Natl. Acad. Sci. USA* **104**, 9182 (2007).
- [21] M. Mezouar, W. A. Crichton, S. Bauchau, F. Thurel, H. Witsch, F. Torrecillas, G. Blattmann, P. Marion, Y. Dabin, J. Chavanne, O. Hignette, C. Morawe, and C. Borel, *J. Synchrotron Radiat.* **12**, 659 (2005).
- [22] A. P. Hammersley, S. O. Svensson, M. Hanfland, A. N. Fitch, and D. Hausermann, *High Pressure Res.* **14**, 235 (1996).
- [23] J. Rodriguezcarvajal, *Physica B* **192**, 55 (1993).
- [24] G. Y. Shen, M. L. Rivers, Y. B. Wang, and S. R. Sutton, *Rev. Sci. Instrum.* **72**, 1273 (2001).
- [25] K. D. Leinenweber, J. A. Tyburczy, T. G. Sharp, E. Soignard, T. Diedrich, W. B. Petuskey, Y. B. Wang, and J. L. Mosenfelder, *Am. Mineral* **97**, 353 (2012).
- [26] P. I. Dorogokupets and A. Dewaele, *High Pressure Res.* **27**, 431 (2007).
- [27] P. Giannozzi, S. Baroni, N. Bonini, M. Calandra, R. Car, C. Cavazzoni, D. Ceresoli, G. L. Chiarotti, M. Cococcioni, I. Dabo, A. Dal Corso, S. de Gironcoli, S. Fabris, G. Fratesi, R. Gebauer, U. Gerstmann, C. Gougoussis, A. Kokalj, M. Lazzeri, L. Martin-Samos, N. Marzari, F. Mauri, R. Mazzarello, S. Paolini, A. Pasquarello, L. Paulatto, C. Sbraccia, S. Scandolo, G. Sclauzero, A. P. Seitsonen, A. Smogunov, P. Umari, and R. M. Wentzcovitch, *J. Phys.-Condens. Mat.* **21**, 395502 (2009).
- [28] J. P. Perdew, K. Burke, and M. Ernzerhof, *Phys. Rev. Lett.* **77**, 3865 (1996).
- [29] K. F. Garrity, J. W. Bennett, K. M. Rabe, and D. Vanderbilt, *Comp. Mater. Sci.* **81**, 446 (2014).
- [30] A. Daoud-Aladine, C. Martin, L. C. Chapon, M. Hervieu, K. S. Knight, M. Brunelli, and P. G. Radaelli, *Phys. Rev. B* **75**, 104417 (2007).
- [31] R. J. Angel, *Rev. Mineral Geochem.* **41**, 35 (2000).
- [32] P. D. Battle, T. C. Gibb, and C. W. Jones, *J. Solid State Chem.* **74**, 60 (1988).
- [33] B. L. Chamberland, A. W. Sleight, and J.F. Weiher, *J. Solid State Chem.* **1**, 506 (1970); K. Kuroda, N. Ishizawa, N. Mizutani, and M. Kato, *J. Solid State Chem.* **38**, 297 (1981).
- [34] O. Chmaissem, B. Dabrowski, S. Kolesnik, J. Mais, D. E. Brown, R. Kruk, P. Prior, B. Pyles, and J. D. Jorgensen, *Phys. Rev. B* **64**, 134412 (2001).
- [35] Y. X. Liu, S. Qin, X. Wu, J. Z. Jiang, K. Takumi, and G. H. Shi, *Chinese Phys. C* **35**, 514 (2011).
- [36] T. Takeda and S. Ohara, *J. Phys. Soc. Jpn.* **37**, 275 (1974).
- [37] D. Fuks, S. Dorfman, J. Felsteiner, L. Bakaleinikov, A. Gordon, and E. A. Kotomin, *Solid State Ionics* **173**, 107 (2004).
- [38] S. Tinte, M. G. Stachiotti, C. O. Rodriguez, D. L. Novikov, and N. E. Christensen, *Phys. Rev. B* **58**, 11959 (1998).
- [39] S. Klotz, J. C. Chervin, P. Munsch, and G. Le Marchand, *J. Phys. D* **42** 75413 (2009).
- [40] R. Mahesh and M. Itoh, *Solid State Ionics* **108**, 201 (1998).